A MULTISCALE MODELING SYSTEM
Developments, Applications, and Critical Issues

BY WEI-KUO TAO, JIUN-DAR CHERN, ROBERT ATLAS, DAVID RANDALL, MARAT KHAIROUTDINOV, JUI-LIN LI, DUANE E. WALISER, ARTHUR HOU, XIN LIN, CHRISTA PETERS-LIDARD, WILLIAM LAU, JONATHAN JIANG, AND JOANNE SIMPSON

NASA's new modeling framework for integrating cloud processes explicitly within each grid column of a general circulation model can improve realism over the conventional model that parameterizes clouds, but it also introduces new biases.

The foremost challenge in parameterizing convective clouds and cloud systems in large-scale models are the many coupled dynamical and physical processes that interact over a wide range of scales, from microphysical scales to the synoptic and planetary scales. This makes the comprehension and representation of convective clouds and cloud systems one of the most complex scientific problems in Earth science. During the past decade, the Global Energy and Water Cycle Experiment (GEWEX) Cloud System Study (GCSS) has pioneered the use of single-column models (SCMs) and cloud-resolving models (CRMs) for the evaluation of the cloud and radiation parame-terizations in general circulation models (GCMs; e.g., GEWEX Cloud System Science Team 1993). These activities have uncovered many systematic biases in the radiation, cloud and convection parameterizations of GCMs and have led to the development of new schemes (e.g., Zhang 2002; Pincus et al. 2003; Zhang and Wu 2003; Wu et al. 2003; Liang and Wu 2005; Wu and Liang 2005, and others). Comparisons between SCMs and CRMs using the same large-scale forcing derived from field campaigns have demonstrated that CRMs are superior to SCMs in the prediction of temperature and moisture tendencies (e.g., Das et al. 1999; Randall et al. 2003b; Xie et al. 2005). This

AFFILIATIONS: TAO, LAU, AND SIMPSON—Laboratory for Atmospheres, NASA Goddard Space Flight Center, Greenbelt, Maryland; CHERN—Laboratory for Atmospheres, NASA Goddard Space Flight Center, Greenbelt, and Goddard Earth Sciences and Technology Center, University of Maryland, Baltimore County, Baltimore, Maryland; ATLAS—NOAA/Atlantic Oceanographic and Meteorological Laboratory, Miami, Florida; KHAIROUTDINOV—Department of Atmospheric Science, Colorado State University, Fort Collins, Colorado; LI, WALISER, AND JIANG—Jet Propulsion Laboratory, California Institute of Technology, Pasadena, California; HOU—Global Modeling and Assimilation Office, NASA Goddard Space Flight Center, Greenbelt, Maryland; LIN—Goddard Earth Sciences and Technology Center, University of Maryland, Baltimore County, Baltimore, and Global Modeling and Assimilation Office, NASA Goddard Space Flight Center, Greenbelt, Maryland; PETERS-LIDARD—Hydrological Sciences Branch, NASA Goddard Space Flight Center, Greenbelt, Maryland
CORRESPONDING AUTHOR: Dr. Wei-Kuo Tao, Code 613.1, NASA Goddard Space Flight Center, Greenbelt, MD 20771
E-mail: Wei-Kuo.Tao-1@nasa.gov

result suggests that CRMs can be important tools for improving the representation of moist processes in GCMs.

Many CRMs use sophisticated and realistic representations of cloud microphysical processes, and they can reasonably well resolve the time evolution, structure, and life cycles of clouds and cloud systems (with sizes ranging from about 2 to 200 km). They also allow for explicit interaction between clouds, outgoing longwave and incoming solar radiation, and ocean and land surface processes. In GCSS-style tests, the CRM results depend strongly on the quality of the input large-scale forcing, and it is difficult to separate model errors from observational forcing errors. Furthermore, offline CRM simulations with observed forcing allow only one-way interaction (from large scale to cloud scale) and cannot simulate the effects of cloud and radiation feedbacks on the large-scale circulation. Recently, Grabowski and Smolarkiewicz (1999), Grabowski (2001), and Khairoutdinov and Randall (2001) proposed a multiscale modeling framework (MMF; previously termed a "superparameterization"), which replaces the conventional cloud parameterizations with a CRM in each grid column of a GCM. In the MMF, a one-dimensional cloud model (or cumulus parameterization) is replaced with a two-dimensional CRM (see Fig. 1; Randall et al. 2003a, their Fig. 16). The MMF can explicitly simulate deep convection, cloudiness and cloud overlap, cloud–radiation interaction, surface fluxes, and surface hydrology at the resolution of a CRM. It has global coverage, and allows for two-way interactions between the CRMs and a GCM. Overviews of this promising approach are given in Randall et al. (2003a)
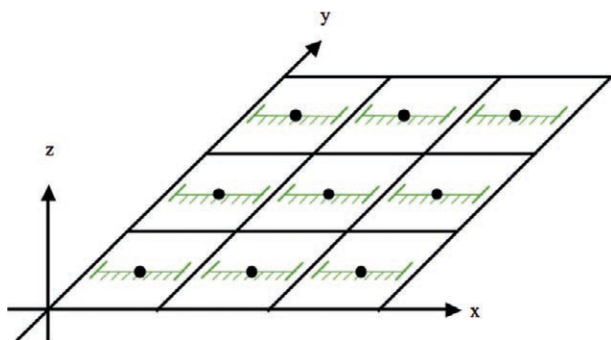

Fig. 1. Current fvMMF grid structure (adopted from Randall et al. 2003a). The black squares represent an array of GCM grid boxes and the lines inside them represent embedded 2D time-variant CRMs. The lateral boundary conditions of the CRM are cyclic (or periodic) and do not extend to the edges of GCM grid boxes. In a traditional GCM, a 1D time-invariant cumulus parameterization is represented by a solid black dot.

and Khairoutdinov et al. (2005). An MMF can be considered as a natural extension of the current SCM and CRM modeling activities of GCSS, the National Aeronautic and Space Administration's (NASA's) Modeling Analyses and Predicting (MAP) program, the U.S. Department of Energy's (DOE's) Atmospheric Radiation Measurements (ARM) Program, and other programs devoted to improving cloud parameterizations in GCMs.

This paper describes the main characteristics of a new MMF developed at the NASA Goddard Space Flight Center (GSFC). The similarities and differences between the Goddard and Colorado State University (CSU) MMFs are briefly described. The performance and application of the two MMFs are analyzed for two simulation years, each having different climate events: the 1998 El Niño and the 1999 La Niña. The Goddard and CSU MMF results and comparisons with satellite observations and those from a GCM using conventional cloud parameterizations are presented. In addition, some critical issues (i.e., the CRM's physical processes and its configuration) associated with the Goddard MMF are discussed.

GODDARD AND CSU MMFS. The Goddard finite-volume MMF (fvMMF hereafter) is based on the NASA Goddard finite-volume GCM (fvGCM) and the Goddard Cumulus Ensemble model (GCE; a CRM). The fvGCM provides global coverage while the GCE allows for the explicit simulation of cloud processes and provides simulated profiles of cloud properties to the fvGCM for handling cloud–radiation interactions. The main characteristics of the fvGCM, GCE, fvMMF, CSU MMF, and their coupling strategy are briefly summarized in the appendix.

There are several differences between the Goddard and CSU MMFs. For example, the Community Atmospheric Model (CAM) in CSU's MMF uses a semi-Largrangian dynamical core in contrast to the finite-volume dynamical core in the Goddard fvGCM. The CSU MMF requires 8,192 CRMs with a T42 (~2.8° × 2.8°) resolution and has 30 vertical layers. For the fvMMF, 12,960 CRMs are required with 2° × 2.5° resolution, and 32 vertical layers are used.[1] The fvGCM uses the National Center for Atmospheric Research (NCAR) Community Climate Model,

---

[1] The computational cost for an MMF is very expensive compared to a traditional GCM with cumulus parameterization. The current Goddard MMF is about 5–10 times more than a 0.25° fvGCM and about the same as a 1/8° fvGCM (Shen et al. 2006a).

TABLE 1. Major characteristics of the MMFs developed at CSU and NASA Goddard. The first three rows are for the corresponding global model and the following six rows the corresponding CRM.

CSU MMF	NASA MMF
CAM (Collins et al. 2006) and CSU/CRM (Khairoutdinov and Randall 2003)	fvGCM (Lin and Rood 1996, 1997) and GCE (Tao et al. 2003)
2.8° × 2.8°, T42 (8,192 CRMs)	2° × 2.5° (12,960 CRMs)
Land surface model (CLM 2)	Modified land surface model (CLM 2; Bloom et al. 2005)
Microphysics (Khairoutdinov and Randall 2003; ~15 processes)	Three microphysics options (Tao et al. 2003; >40 processes)
1.5-order TKE (Khairoutdinov and Kogan 1999)	1.5-order TKE (Soong and Ogura 1980)
NCAR CAM radiation (Collins et al. 2006)	Goddard radiation (Chou and Suarez 1999, 2001)
Time step (20 s)	Time step (10 s)
CRM has 32 columns with 28 vertical layers oriented in north–south direction (Khairoutdinov et al. 2008)	CRM has 64 columns and 30 vertical layers oriented in east–west direction
None	In-line cloud statistics (every 2 min)
24 h per simulated year on a 1024-CPU computer	365 h per simulated year on a 384-CPU computer

version 3 (CCM3) physics,[2] while the CSU MMF uses the NCAR CAM physics.

The CRMs used in the CSU and Goddard MMFs both apply an anelastic approximation and positive definite monotonic advection schemes. For subgrid-scale motion, a prognostic 1.5-order turbulent kinetic energy (TKE) scheme is used in both CRMs; the Goddard CRM also includes the effects of condensation on the generation of subgrid-scale kinetic energy and a stability dependence on the dynamic and scalar turbulence coefficients. The CRM used in the CSU MMF has a relatively simple microphysics package with 15 processes governing the interaction between hydrometeors and water vapor (Khairoutdinov and Randall 2003); the GCE model (Tao et al. 2003) has more than 40 parameterized microphysical processes. The CRM time step used in the CSU and Goddard MMF is also different. The Goddard CRM has in-line cloud statistics to record the cloud properties in the convective and stratiform regions, convective updrafts, convective downdrafts, and the apparent heat (Q_1) and apparent moisture (Q_2) budgets (see Tao et al. 1987). More CRMs (12,960 versus 8,192), more CRM columns (64 versus 32), a smaller time step (10 versus 20 s), and in-line cloud statistics (every minute) in the Goddard MMF increase the computational requirements compared to the CSU MMF. Table 1

compares the main characteristics of the Goddard and CSU MMFs.

RESULTS. *Performance of the Goddard MMF and comparison with satellite observations.* The Goddard MMF has been evaluated against observations at interannual, intraseasonal, and diurnal time scales using a 2-yr-long simulation representing different climate scenarios, namely, the 1998 El Niño and the 1999 La Niña. The model was forced by the observed National Oceanic and Atmospheric Administration (NOAA) optimal interpolation (OI) weekly sea surface temperatures (SSTs; Reynolds et al. 2002), and the initial conditions for the two simulations came from the Goddard Earth Observing System, version 4 (GEOS-4; Bloom et al. 2005) analyses at 0000 UTC 1 November 1997 and 1998, respectively. Similar runs with the same initial conditions and SSTs were performed using the fvGCM with the traditional parameterization of moist processes (i.e., NCAR CCM3 physics; Kiehl et al. 1998). Both fvMMF and fvGCM runs have the same horizontal and vertical resolution (2° × 2.5° in the horizontal and 32 layers in the vertical).

Figures 2 and 3 show the geographical distribution of simulated precipitation for January and July of 1998 and 1999 from the fvGCM, fvMMF, and CSU MMF, along with the corresponding observations from the Tropical Rainfall Measuring Mission (TRMM; Simpson et al. 1988, 1996) Microwave Imager (TMI; Kummerow et al. 2001). In general, given the observed SST forcing, the observed patterns of monthly mean precipitation can be realistically simulated by the

---

[2] Community Land Model version 2 (CLM2; Bonan et al. 2002; Oleson et al. 2004) is used in both the fvGCM and CAM, except that the CLM used in the fvGCM includes a number of significant modifications made at NASA GSFC (Bloom et al. 2005).
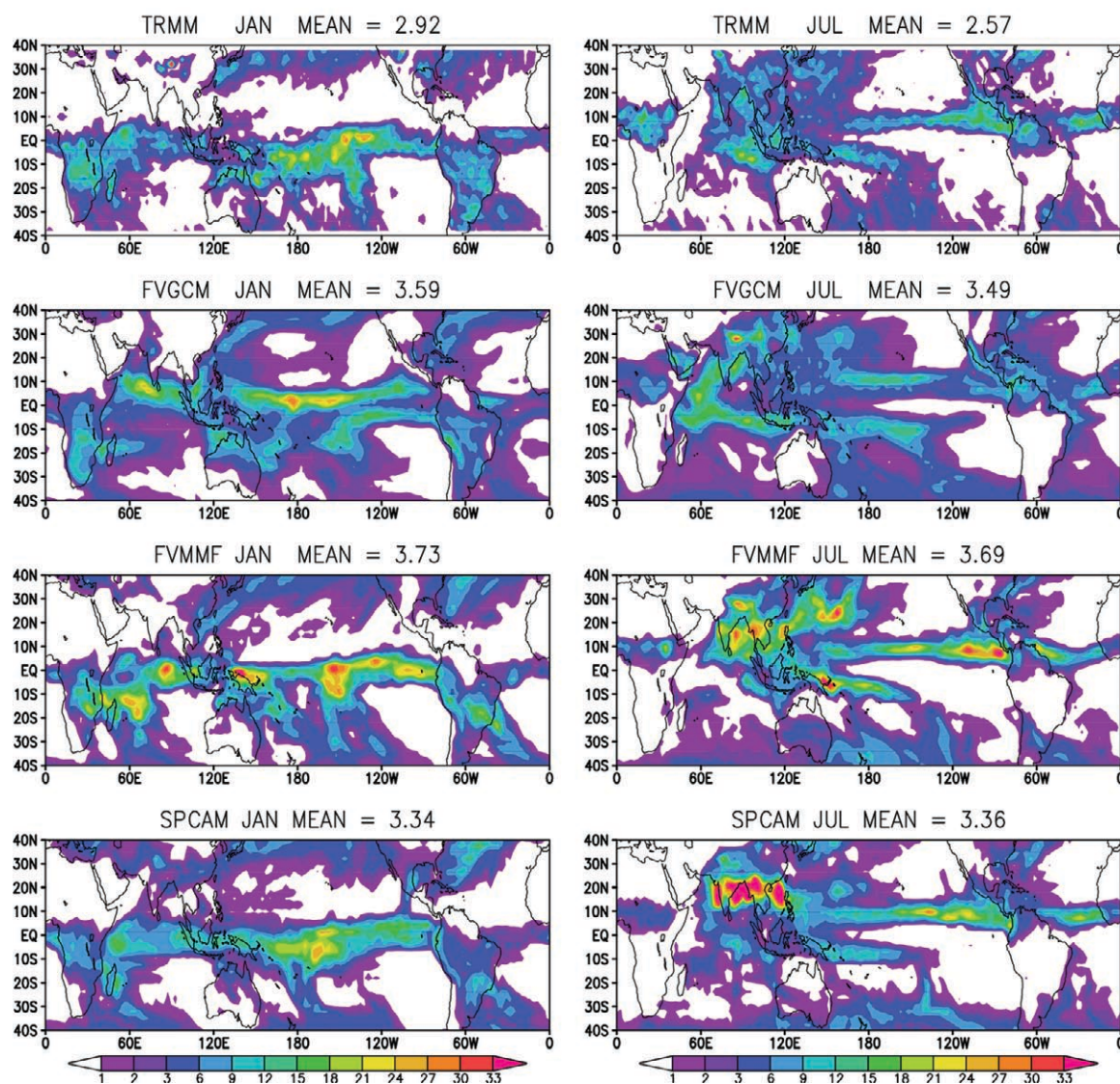
FIG. 2. Monthly precipitation rate (mm day^{-1}) from the (from top to bottom) TMI, fvGCM, Goddard MMF, and CSU MMF for (left) Jan 1998 and (right) Jul 1998. Note that the original TMI rainfall dataset at 0.5° resolution has been averaged to the fvGCM grid size.

MMFs and fvGCM for extratropical storm tracks and the tropics. The shift in tropical precipitation to the central Pacific in January 1998 during El Niño is well captured. The intertropical convergence zone (ITCZ), the South Pacific convergence zone (SPCZ), and the South Atlantic convergence zone (SACZ) are also well reproduced. The precipitation patterns and dry areas for both MMFs tend to be slightly more realistic than those of the fvGCM; in particular, the unrealistic double ITCZ simulated by the fvGCM for July 1998 and 1999 is not present in the MMFs.

There are apparent biases in the fvMMF, however. For example, monthly mean precipitation averaged over the tropics is about 30% (4%–6%) more than the TRMM observations (fvGCM) in both winter and summer. The fvMMF precipitation in the western Pacific, eastern tropical Pacific, Bay of Bengal, and western India Ocean is too high during summer; a similar phenomenon occurs in simulations with the CSU MMF (Khairoutdinov et al. 2005; Figs. 2 and 3). It is remarkable that both MMFs exhibit the same precipitation bias despite the many differences in their GCM dynamical cores and CRM microphysics parameterizations (Table 1). Because of the nonlinear coupling between the GCM and the CRM, the physical cause(s) of the positive precipitation bias is (are) very
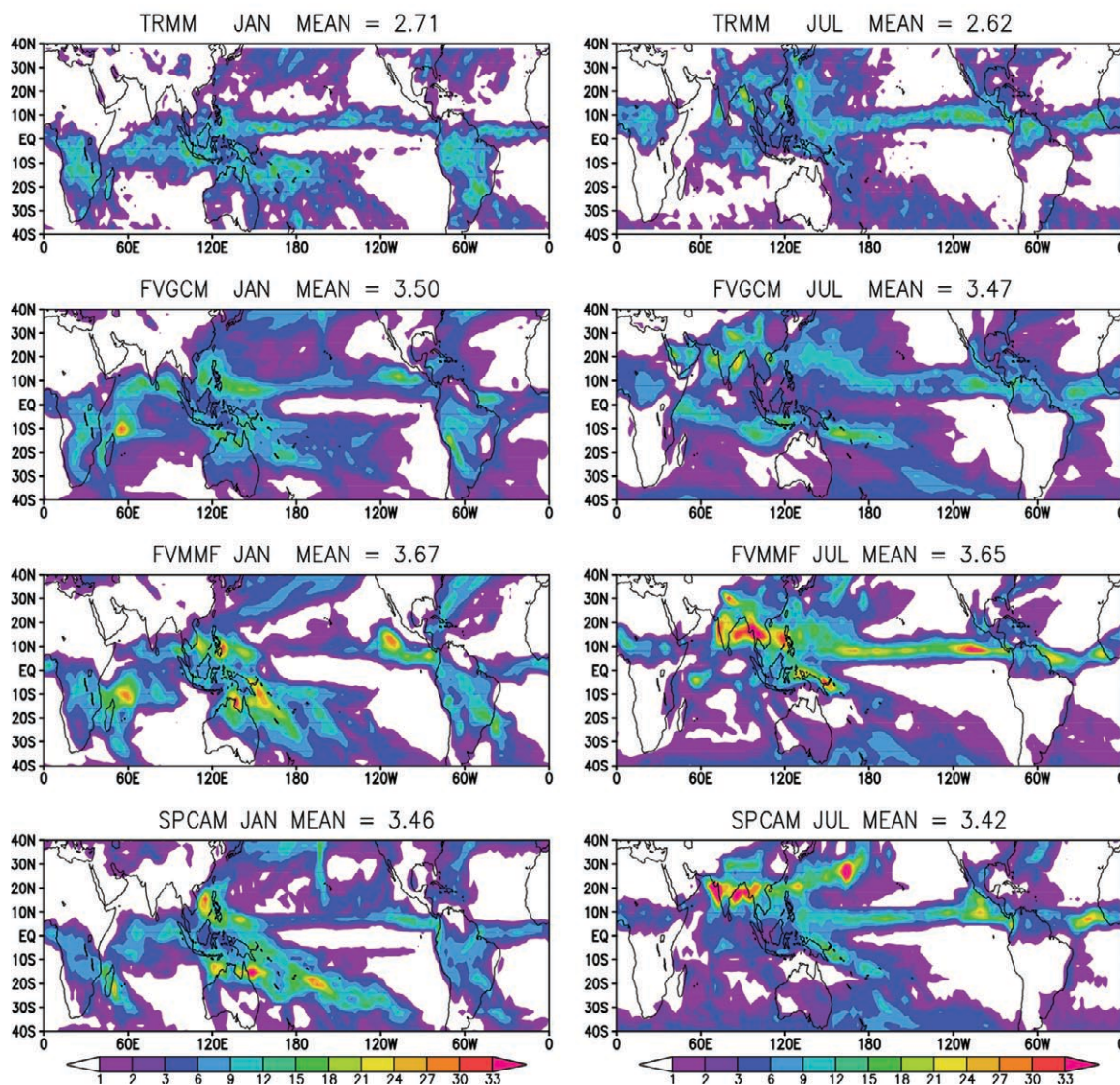
Monthly Precipitation Rate (mm/day) 1999

FIG. 3. Same as Fig. 2, except for the year 1999.

difficult to isolate and identify. The use of 2D CRMs with cyclic lateral boundary conditions, which do not allow deep convective systems to propagate to the neighboring GCM grid boxes, is believed to be one of the causes of the precipitation bias (Khairoutdinov et al. 2005). Luo and Stephens (2006) suggested that the cyclic boundary conditions of the CRM lead to an artificial trapping of convection at the CRM level and a prolonged lifetime. This trapping leads to excessive cloud latent heat release, which forces anomalously strong winds at the GCM level. Enhanced surface winds then increase surface evaporation. Finally, the enhanced evaporation and surface winds feed back to fuel the convection at the CRM level by enhancing moisture convergence.[3] However, Khairoutdinov et al. (2005) have demonstrated that the precipitation bias can be improved with a 3D CRM (using a small domain, 8×8 grid points), especially when convective momentum transport is included. Their study suggests that dimensionality (2D versus 3D CRM) and sampling in one direction might be the cause of the precipitation bias.

---

[3] Luo and Stephens (2006) referred to this process as "*convection–wind–evaporation*" feedback. Note that the convection–wind–evaporation feedback operates at the GCM scale because surface latent heat flux is evaluated at the GCM scale in the current MMF.

Vertical velocities simulated by the fvMMF are considerably stronger (resulting from CRM-simulated latent heat release), particularly over the tropical region, than those in the fvGCM. This may be another factor in producing the active precipitation (bias) and could also explain why there is more precipitation in the fvMMF than fvGCM. Furthermore, the compensating downward motion is also stronger and produces stronger warming and drying in the fvMMF. The strong convection-induced subsidence causes the fvMMF to simulate larger and more realistic nonraining regions.

Recently, Wu et al. (2007) examined the effect of convective momentum transport on global climate simulations. Their results suggested that the coupling of convective momentum transport with convective heating could weaken equatorial convergence and convection. Sensitivity tests will be required to examine the impact of convective momentum transport in the GCM used in the MMF on the positive precipitation bias over the western Pacific, eastern tropical Pacific, Bay of Bengal, and western India Ocean.

Figure 4 shows probability distribution functions (PDFs) of ice water content (IWC) at 147 hPa based on Microwave Limb Sounder (MLS) retrievals version 1.5 for January 2005 and for the period from August 2004 to July 2005, as well as hourly instantaneous values of IWC (not including precipitating ice) from the fvMMF and CSU MMF for January 1998. The PDFs for a complete year and a single month of MLS data suggest that a month of sampling provides a good representation of the overall occurrence frequencies. The MLS-retrieved annual (red bars) and January (dark blue bars) PDFs are quite similar and suggest that a month of sampling reasonably well represents the overall occurrence frequency when the entire globe is considered. In addition, the PDFs clearly illustrate the lower and upper limits of the MLS sensor's sensitivity at this pressure level, about 0.4 and 40 mg m^{-3}, respectively. Overall, both MMFs show good agreement in terms of the shape of the distribution with the MLS IWC observations between the range of 0.5 and 30 mg m^{-3}. The CSU MMF has a slightly higher frequency of occurrence than the fvMMF at lower (<5 mg m^{-3}) and higher IWCs (>35 mg m^{-3}). The large IWCs (>25.0 mg m^{-3}) simulated by the Goddard MMF occur mainly over either continents or coasts except for in the central and eastern Pacific during January 1998. Large vertical cloud velocities associated with storms that developed over land and coastal areas is the main cause for the larger IWCs [convective available potential energy (CAPE) is larger over land than ocean]. For January 1998, deep convective systems responding to the warm SSTs in the central and eastern Pacific produce large amounts of ice aloft. Similar results can be found for July 1998 and January and July 1999 (not shown).

The Madden–Julian oscillation (MJO; Madden and Julian 1972, 1994) is one of the most prominent large-scale features of the tropical general circulation. While the MJO is evident in circulation fields throughout the tropics (Madden and Julian 1972; Knutson and Weickmann 1987), it is typically characterized by deep convection originating over the Indian Ocean and subsequent eastward propagation into the Pacific Ocean. Figure 5 shows Hovmöller diagrams of the daily tropical precipitation rate averaged between 10°S and 10°N from the Global Precipitation Climatology Project (GPCP), fvGCM, fvMMF, and CSU MMF for 1998 and 1999. The fvGCM and MMFs realistically reproduce the El Niño–associated eastward shift in the broad envelope of
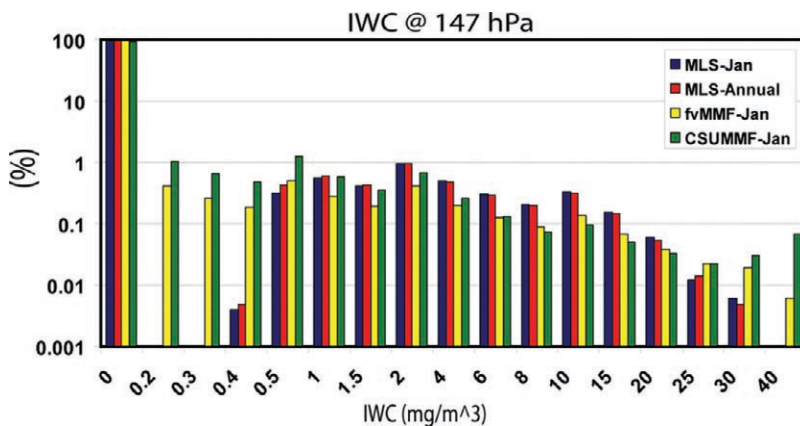

FIG. 4. Probability distribution functions of MLS IWC (mg m^{-3}) at 147 hPa for Jan 2005 (dark blue bars) and for the period from Aug 2004 to Jul 2005 (red bars), along with model results from the fvMMF (yellow bars) and CSU MMF (green bars) for Jan 1998. The spatial resolution of the MLS sampling and the MMFs is not identical but quite similar. The MLS data are based on the inherent sensor footprint [a cigar-shaped pixel represents an observed mean quantity over a volume of about 300 km × 7 km × 4 km (length × width × height) at the 147-hPa level]. The modeled IWC at each GCM grid is the mean IWC (not including precipitating ice) of the 64 grid points of the embedded 2D CRM. It represents an average IWC over a volume of about 256 km × 4 km × 1 km.
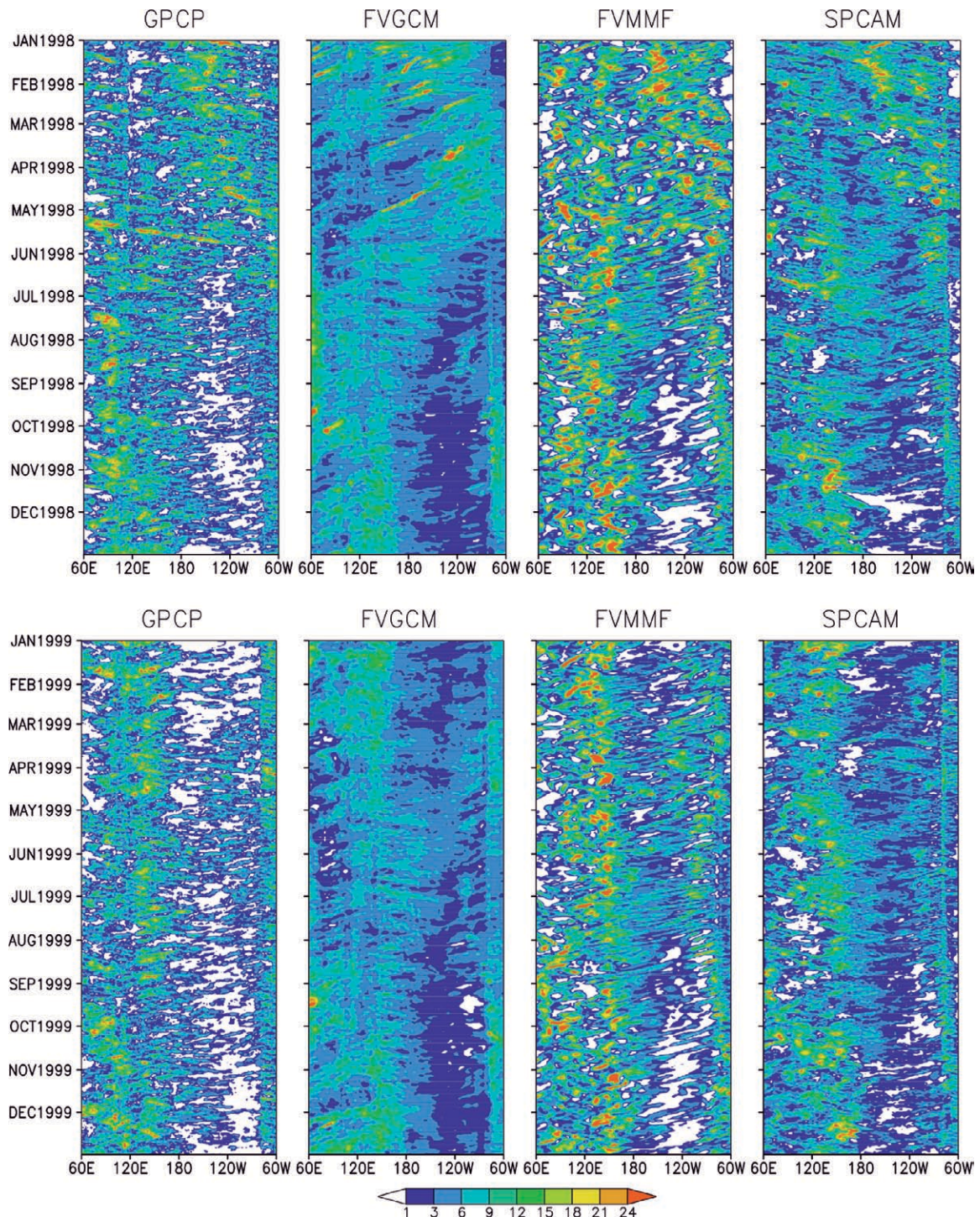
FIG. 5. Hovmöller diagrams of tropical (averaged from 10°S to 10°N) daily precipitation rate (mm day⁻¹) for the (from left to right) GPCP, fvGCM, fvMMF, and CSU MMF (top) from 1 Jan 1998 to 31 Dec 1998 and (bottom) from 1 Jan 1999 to 31 Dec 1999.

convection from the western Pacific warm pool to the eastern Pacific during winter 1997 and spring 1998 and the westward shift after summer 1998. During the 1999 La Niña, the broad-scale deep convective rain remains over the western Pacific warm pool

region. Overall, the MMFs (fvGCM) tend to produce stronger (weaker) convective precipitation than that observed. Superimposed on the broad interannual patterns, the MMFs show vigorous convection propagating eastward. In contrast, the fvGCM run

only shows some westward-propagating convection signals; the eastward-propagating MJO signals are virtually nonexistent. These results are consistent with the earlier findings (e.g., Grabowski 2003; Randall et al. 2003a) that MMFs can more realistically simulate the tropical intraseasonal oscillation than GCMs with conventional cloud parameterizations. However, it is still not clear what major physical processes are associated with the improved MJO signal in the MMF. One possible reason for the improved
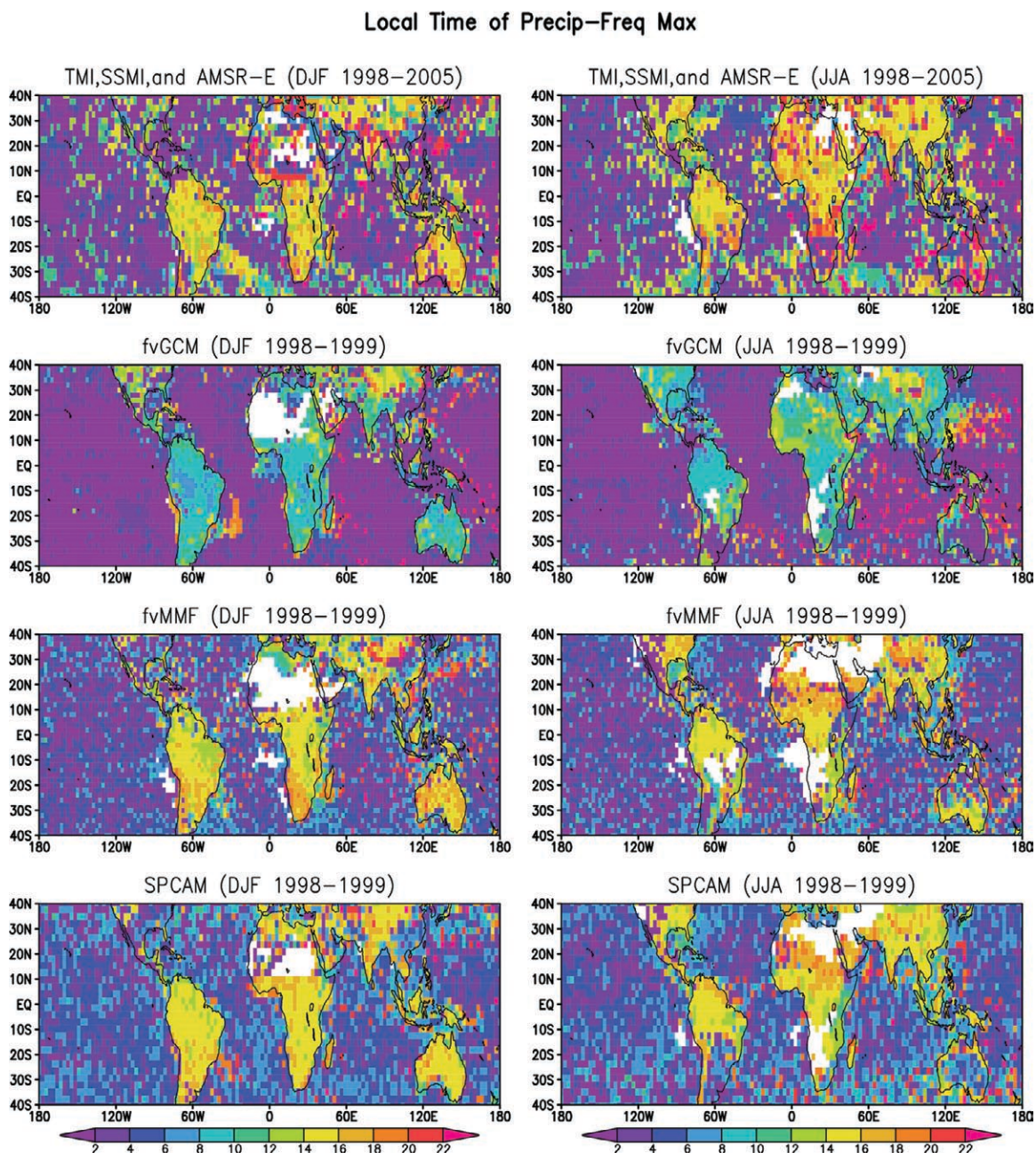

Fig. 6. Geographical distribution of the LST for the nondrizzle precipitation frequency maximum in (left) winter and (right) summer as (from top to bottom) observed by satellite from 1998 to 2005, simulated with the Goddard fvGCM, Goddard MMF, and CSU MMF for 2 yr (1998 and 1999). Blank regions indicate no precipitation. The MMF results are based on detailed 2D GCE model-simulated hourly rainfall output. Satellite-retrieved rainfall is based on a five-satellite constellation, including the TMI, Special Sensor Microwave Imager (SSM/I) from the Defense Meteorological Satellite Program (DMSP) F13, F14, and F15; and the Advanced Microwave Scanning Radiometer Earth Observing System (AMSR-E) on board the *Aqua* satellite.

MJO simulations may be due to better synoptic-scale weather systems (i.e., precipitation patterns and distributions) in the MMF (Khairoutdinov et al. 2008). The positive precipitation bias in the MMFs might be the reason for the stronger MJO.

The diurnal cycle is a fundamental mode of atmospheric variability. Successful simulation of the diurnal variability of the hydrologic cycle and radiative energy budget provides a robust test of physical processes represented in atmospheric models (e.g., Slingo et al. 1987; Randall et al. 1991; Lin et al. 2000; Yang and Slingo 2001; Betts and Jakob 2002; Guichard et al. 2004). Figure 6 shows the geographical distribution of the local solar time (LST) of the nondrizzle precipitation frequency maximum in winter and summer of 1998 as simulated by the fvGCM, fvMMF, and CSU MMF. Satellite microwave rainfall retrievals from a five-satellite constellation are analyzed at 1-h intervals from 1998 to 2005 for comparison. The nondrizzle precipitation is defined as precipitation that occurs such that the 1-h averaged rain rate is larger than 1 mm day^{-1} (see Lin et al. 2007).

Satellite microwave rainfall retrievals in general show that precipitation occurs most frequently in the afternoon to early evening over the major continents such as South and North America, Australia, and west and central Europe, reflecting the dominant role played by direct solar heating of the land surface. Over open oceans, a predominant early morning maximum in rain frequency can be seen in satellite observations, consistent with earlier studies (Sui et al. 1997, 2008). It is again remarkable that both MMFs are superior to the fvGCM in reproducing the correct timing of the late afternoon and early evening precipitation maximum over land and the early morning precipitation maximum over the oceans. The fvGCM, in contrast, produces a dominant morning maximum

rain frequency over major continents. Additional and more detailed comparisons between the observed and MMF-simulated diurnal variation of radiation fluxes, clouds, and precipitation under different large-scale weather patterns and different climate regimes will be published elsewhere.

Comparison of the Goddard and CSU MMFs. Despite differences in model dynamics and physics between the Goddard and CSU MMFs, both simulate stronger MJOs and a more realistic diurnal variation of rainfall than traditional GCMs. Both MMFs also have similar model biases, such as the precipitation bias problem, compared to observations and the parent GCMs. All of the model runs (i.e., from the two GCMs and the two MMFs) overestimate global rainfall compared to satellite estimates for 1998 (El Niño) and 1999 (La Niña; Table 2). Both MMFs also overpredict the total oceanic surface rainfall compared to observations and their parent GCMs (Table 3). Note that the Goddard MMF simulated more rainfall than its parent GCM for both years. In contrast, the CSU MMF simulated less rainfall than its parent GCM over land. However, the CSU MMF and its GCM (CAM)-simulated rainfall are in better agreement with satellite estimates than the fvMMF and fvGCM for both years.

It might be expected that the MMF-simulated rainfall would be close to that of its parent GCM because many of the key physical processes (i.e., surface processes, radiation, and prescribed SSTs) in the MMFs are identical to those in the GCMs (see Table 2). In addition, the key coupling strategy or design of the MMF is not to allow the MMF's mean field to systematically "drift" away from the corresponding GCM fields (see Khairoutdinov et al. 2005, and their section 2.4).

TABLE 2. The global annual mean rainfall rate (mm day^{-1}) for 1998 and 1999 from the fvGCM, fvMMF, CAM, and CSU MMF. The observed rainfall (GPCP V3) is also shown for comparison.

	Observation	fvGCM	fvMMF	CAM	CSU MMF
1998	2.65	3.07	3.17	2.88	2.84
1999	2.59	3.05	3.14	2.83	2.81

TABLE 3. Same as Table 2, except showing rainfall over ocean and land.

	Observation	fvGCM	fvMMF	CAM	CSU MMF
1998 (ocean)	2.92	3.43	3.55	3.08	3.15
1998 (land)	2.02	2.21	2.27	2.38	2.06
1999 (ocean)	2.80	3.38	3.52	3.04	3.15
1999 (land)	2.09	2.26	2.25	2.34	1.98

Both MMFs overestimate oceanic rainfall (2%–3%) compared to their parent GCMs and satellite estimates for both years (Table 3). The CSU MMF simulated less rainfall over land than its parent GCM. This is why the CSU MMF simulated less global rainfall than its parent GCM (Table 2). The fvMMF overestimates global rainfall because of its oceanic component. The CSU MMF simulated the same amount of oceanic rainfall in both 1998 and 1999, implying that the CSU MMF is more sensitive to its land processes than its oceanic processes. The fvMMF shows more variation in rainfall over ocean than land between 1998 and 1999. Note that the CSU MMF-simulated global rainfall amount agrees better with satellite estimates.

Geographical distributions of the annual mean high cloud amount from the International Satellite Cloud Climatology Project (ISCCP) observations, fvGCM, fvMMF, and CSU MMF are shown in Fig. 7. The fvMMF and CSU MMF cloud fractions are derived from the embedded CRMs, assuming it is either clear or overcast depending on cloud ice and liquid water amount, and then averaged to the GCM grid box. It should be noted that cloud ice water optical depth is used in the CSU MMF and cloud ice and cloud water mixing ratio in the fvMMF to detect clouds in their respective CRMs. Both MMFs are able to simulate the global distribution of high cloud amount rather well. On the other hand, the

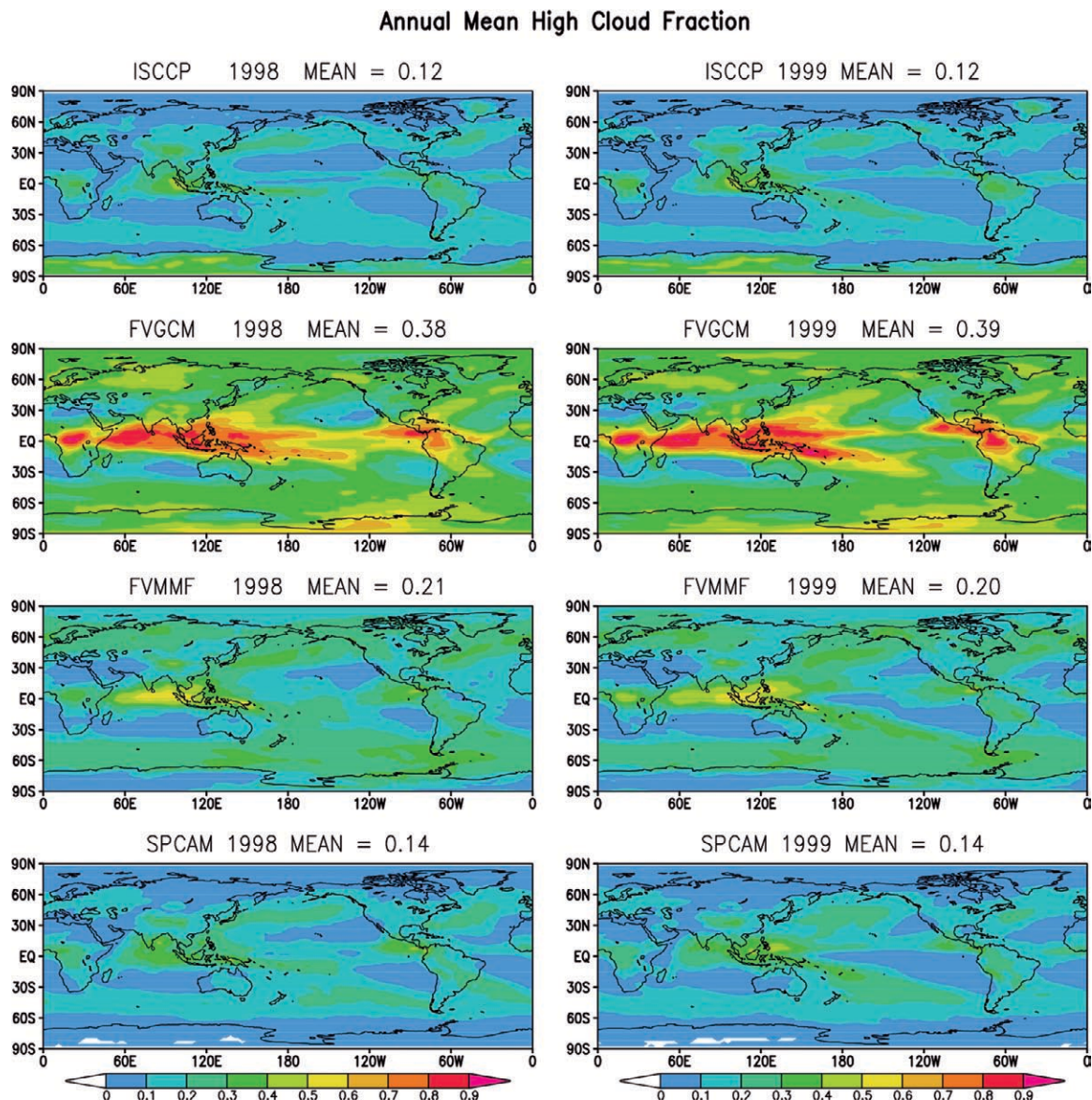## Annual Mean High Cloud Fraction

FIG. 7. Annual mean high (above 400 hPa) cloud fractions from (from top to bottom) ISCCP observations, the fvGCM, fvMMF, and CSU MMF for (left) 1998 and (right) 1999.

fvGCM tends to significantly overestimate high cloud. Because all of the models and the satellite observations show almost identical global mean high, middle, and low cloud amounts, respectively, for 1998 and 1999, only the cloud amounts for 1998 are shown in Table 4. Both of the MMFs exhibit much better agreement with ISCCP cloud amounts (especially high and low) than do the GCMs. The CSU MMF-simulated high cloud amount agrees best with the satellite estimate.

Cloud radiative effects are best illustrated by shortwave cloud forcing (SWCF) and longwave cloud forcing (LWCF), which is the difference between the clear-sky and total radiative fluxes at the top of the atmosphere. The global distributions of 2-yr (1998–99)-averaged SWCF and LWCF from the International Satellite Cloud Climatology Project (ISCCP) Flux Data (FD) observational estimate dataset (Zhang et al. 2004) and the fvGCM, fvMMF, and CSU MMF simulations are shown in Fig. 8. The global mean values for both MMFs agree better than those of the fvGCM with the ISCCP-FD estimates. However, there are still large regional biases in both MMFs. The large positive (negative) biases of longwave (shortwave) cloud forcing in the tropics are well correlated with the positive precipitation biases and overestimates of high cloud amount in the tropics. The large positive SWCF biases are consistent with the underestimates of low cloud amount west of subtropical continents where stratocumulus clouds are frequently located. Of note, the fvMMF was not intentionally tuned to balance global energy. For the rather short 2-yr simulation, the average energy unbalance at the model top and surface were 1.96 and 1.15 W m^{-2}, respectively, which is considered reasonably small for an unturned global model.

ISSUES AND FUTURE RESEARCH. The MMF approach is extremely computer intensive and can produce immense datasets. In this paper, only the variables and features inherent in their parent GCMs are compared. To fully understand the strengths and weaknesses of the MMF approach in climate modeling, a more detailed comparison

between the two MMFs for longer simulations (i.e., 10-yr integrations or longer), including simulated cloud properties from their CRM components as well as their improvements and sensitivities (see this section), will be needed. Through the National Science Foundation (NSF)-funded Science and Technology Center [known as the Center for Multi-Scale Modeling of Atmospheric Processes (CMMAP) at CSU], the developers of the Goddard and CSU MMFs are in the process of conducting a more detailed evaluation of the MMFs' performance against satellite and ground-based observations (to be presented in a future paper).

There are still many critical issues related to the MMF that need additional exploration and diagnosis that may have a major impact on MMF performance. Specifically, the grid configuration of the CRMs within the MMF and the assumptions/physics used in the CRMs need to be addressed. The lifetime of convective cloud systems is usually greater than 1 h. As such, a longer coupling/communication time between the CRM and GCM may be needed.

Configuration of CRMs within the MMF. The potential weaknesses of the current framework are as follows: 1) use of a 2D version of CRMs, 2) use of a cyclic lateral boundary conditions in the CRM, 3) communication between neighboring CRMs through the GCM, 4) use of coarse vertical and horizontal grid sizes in the CRM (4 km for the present study), 5) use of one single type of bulk microphysics for all types of clouds/convective systems developed in different geographic locations and seasons, parameterizations for cloud–radiation interactions, and subgrid-scale turbulent processes in the CRM, 6) the absence of land surface and terrain effects in the CRMs, and 7) the lack of the dynamic (i.e., momentum) feedbacks/interactions between the CRM and GCM. Some of critical issues can be addressed by the quasi-3D approach (Randall et al. 2003a; Arakawa 2004; see Fig. 9a). However, the quasi-3D approach is more difficult to implement and more expensive computationally. At Goddard, an MMF based on a global 2D CRM (see Fig. 9b) is also being developed to address some of these issues.

TABLE 4. High, middle, and low cloud amounts simulated from the fvGCM, Goddard MMF, CAM, and CSU MMF. Observed cloud amounts are shown for comparison.

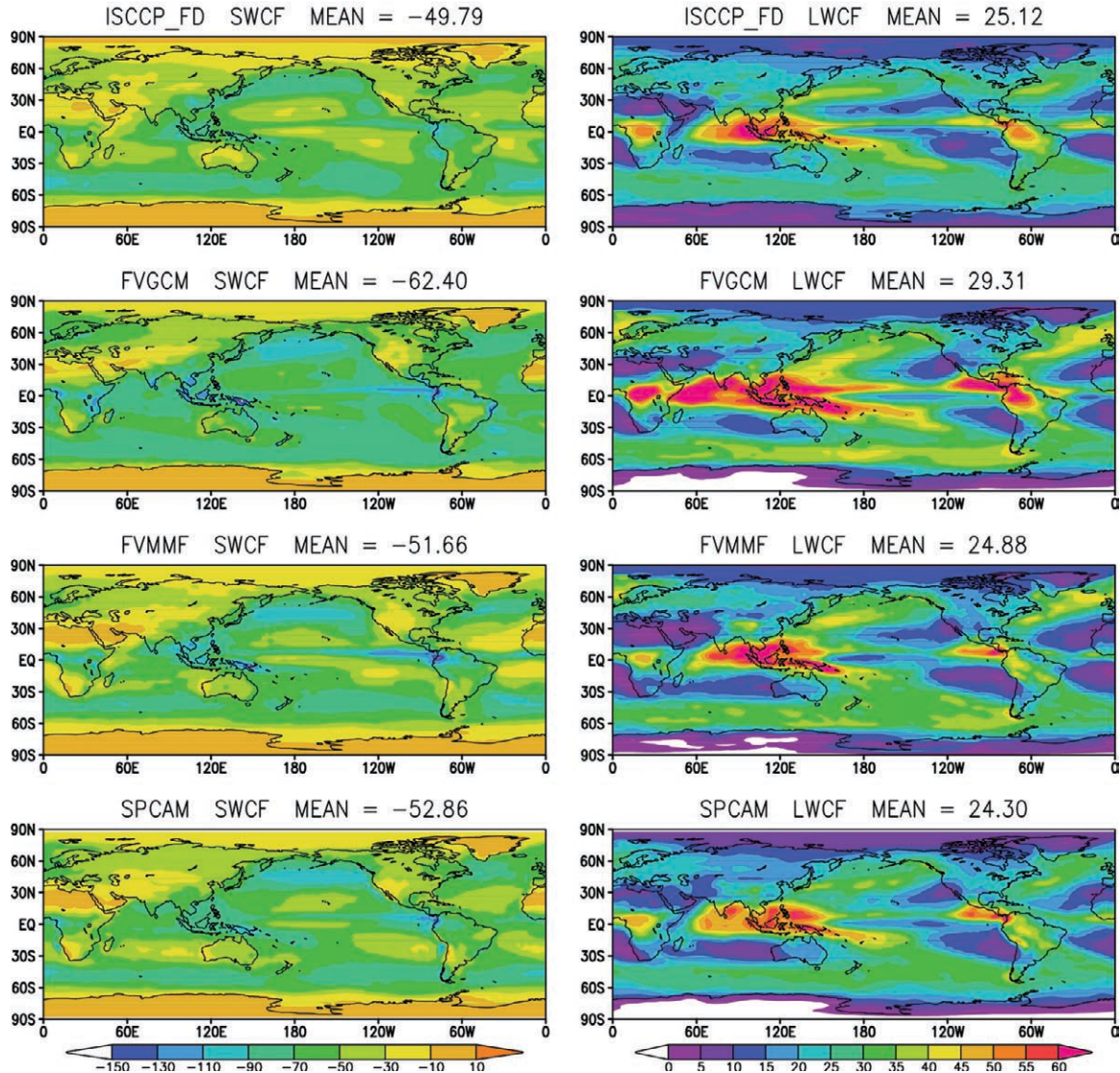|	Observation	fvGCM	fvMMF	CAM	CSU MMF
1998 high cloud amount	0.12	0.38	0.21	0.36	0.14
1998 middle cloud amount	0.20	0.21	0.17	0.21	0.15
1998 low cloud amount	0.27	0.45	0.35	0.43	0.33

Mean Cloud Forcing at TOA (W/m2)

Fig. 8. Two-year (1998–99) averaged (left) shortwave and (right) longwave cloud forcing (W m⁻²) at the top of the atmosphere (TOA) from (from top to bottom) ISCCP-FD observational estimates, the fvGCM, fvMMF, and CSU MMF simulations.

Issues related to the CRM used in the MMF. Some of the deficiencies in the current MMF are related to the dynamic and physical processes used in the CRM. These issues can be studied either by using the MMF itself or through the use of offline 2D and/or 3D CRMs.

DIMENSIONALITY (2D VERSUS 3D). Real clouds and cloud systems are 3D. Because of the limitations of computer resources, a 2D CRM is being used in the MMF. Previous cloud modeling studies (e.g., Tao and Soong 1986; Lipps and Hemler 1986; Tao et al. 1987; Grabowski et al. 1998; Khairoutdinov and Randall

2001; Zeng et al. 2007, and others) have addressed the modeling dimensionality issues. However, these modeling studies showed very different results. For example, Grabowski et al. (1998) found that cloud statistics as well as surface precipitation were significantly different between their 2D and 3D simulations of tropical convection. However, Khairoutdinov and Randall (2001) and Zeng et al. (2007) found that surface rainfall is not very sensitive between 2D and 3D model simulations for midlatitude cases.

Recently, Khairoutdinov et al. (2008) applied their 2D CRM with a north–south orientation instead of an east–west alignment (Khairoutdinov et al. 2005) in
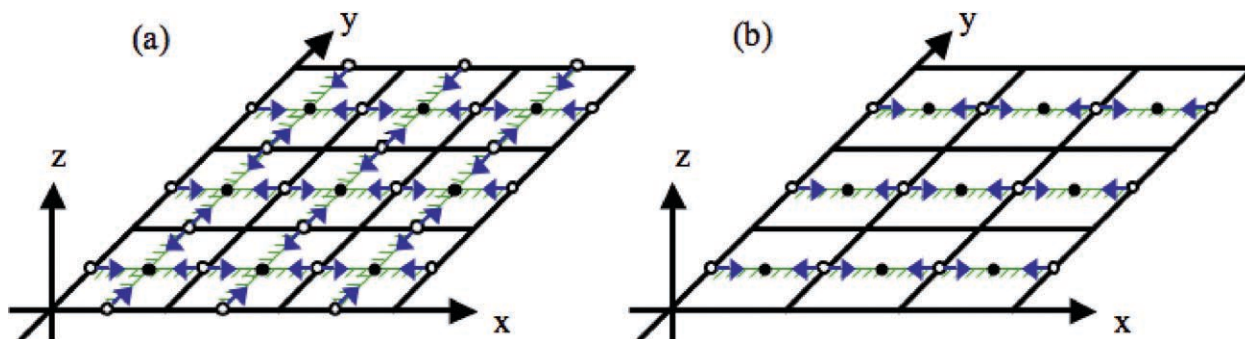
FIG. 9. (a) A quasi-3D CRM structure (from Randall et al. 2003a). Here the two orthogonal high-resolution CRM grids are extended to the walls of the GCM grid cells. (b) A global 2D CRM structure (single east–west orientation). In both new approaches, cyclic lateral boundary conditions are replaced by direct coupling of the CRMs in neighboring GCM cells, as depicted by the arrows. The effects of topography may be required in the embedded CRMs.

the CSU MMF. They found that it seems to mitigate the excessive precipitation in the western Pacific for the summer months. The underlying physical processes for the improvement are not yet understood. When the CRM domain alignment is changed, the corresponding mean state and constraints of the CRM mean wind also change (i.e., from zonal wind in the east–west orientation to meridional wind in the north–south alignment). Because there is no momentum feedback and explicit coupling between surface processes and their CRM in the CSU MMF, the improvement may be due to the change of mean vertical wind shear. Low-level vertical wind shear is well known to be crucial for cloud development and mesoscale organization. Additional tests comparing 2D CRM simulations using different east–west and south–north configurations and 3D CRM simulations using the fvMMF are still needed.

Anelastic versus compressible. The CRM dynamics can be either anelastic (Ogura and Phillips 1962), filtering out sound waves, or compressible (Klemp and Wilhelmson 1978), allowing sound waves. The sound waves are not important for thermal convection, but because of their high propagation speed, they create severe restrictions on the time step used in numerical integrations. For this reason, most cloud models (including those used in the Goddard and CSU MMFs) use an anelastic system of equations. To be consistent with the dynamics of the host fvGCM, a compressible dynamical core is required. Results from a 1-month fvMMF simulation indicate that using a compressible system in the GCE results in better precipitation amounts and patterns (rainfall associated with the Asian summer monsoon is reduced), in terms of bias and root-mean-square error compared to the

anelastic approach. The cause(s) of these differences is (are) currently under investigation.

Microphysics. Both the Goddard and CSU MMF use a one-moment bulk microphysical scheme (e.g., the three ice hydrometeors (3ICE) scheme with cloud ice, snow and graupel) for all clouds and cloud systems. Typically, graupel is used as the third class of ice when simulating tropical oceanic systems while hail is used to simulate midlatitude continental systems (McCumber et al. 1991; Tao et al. 1996). Therefore, sensitivity tests are required to examine the impact of different bulk microphysical schemes (e.g., 3ICE with graupel, 3ICE with hail) in the MMF. By comparing model results with observations, errors in the simulated hydrometeor fields can be investigated, identified, documented, and improved, especially in regards to uncertainties often associated with the cloud microphysical schemes (i.e., Lang et al. 2007). The effects of aerosols should also be tested with advanced microphysical schemes (i.e., spectral bin microphysics or a multimoment scheme).

Land surface. Interactions between the atmosphere and the land surface have considerable influence on local, regional, and global climate variability. Therefore, coupled high-resolution land–atmosphere systems (i.e., Kumar et al. 2006) that can realistically represent these interactions are critical for improving our understanding of the atmosphere–biosphere exchanges of water, energy, and their associated feedbacks. How to represent observed heterogeneities in land characteristics (i.e., soil, vegetation) in 2D (with cyclic lateral boundary conditions) could be a major issue for MMFs. The simplest method is a random distribution (Zeng et al. 2007). A more

physical approach is to use PDF matching between observed surface fluxes (or land characteristics) and modeled surface properties (i.e., the product of wind stress and air–land temperature/moisture differences, or rainfall). Both methods will be tested to improve the MMF's ability to represent these processes and to identify the key land–atmosphere feedbacks and their impact on the local and regional water and energy cycles.

BOUNDARY LAYER SCHEME. While large cloud (or convective) eddies are resolved in CRMs, eddies smaller than the gridscale must still be parameterized. An assumption is that all turbulent motions are subgrid scale (SGS), and hence an ensemble mean turbulence model is often used to represent the net effect of unresolved turbulence. The current CRMs embedded in the MMF applied the TKE equation (1.5 order) prognostically. In the prognostic TKE method, thermodynamic stability, deformation, shear stability, diffusion, dissipation, moist processes, and the transport of subgrid energy are included (Klemp and Wilhelmson 1978).

A higher-order turbulence approach would be necessary to simulate realistic shallow cumuli and boundary layer cumulus (i.e., Cheng and Xu 2006). It is unclear to what extent 2D CRMs properly represent large convective eddies, which in nature are three-dimensional. A comprehensive study of the effect of planetary boundary schemes on shallow convection is needed.

SUMMARY. The idea for the MMF, whereby conventional cloud parameterizations are replaced with CRMs in each grid column of a GCM, was proposed by Grabowski and Smolarkiewicz (1999) and Grabowski (2001). Khairoutdinov and Randall (2001) and Randall et al. (2003a) developed the first MMF based on a GCM developed at NCAR (CAM) and a CRM at CSU. A second, more recent MMF based on the fvGCM and the GCE has been developed. This Goddard MMF's performance was evaluated and compared against satellite observations, its parent GCM (fvGCM), and the CSU MMF for 2-yr-long simulations representing different climate scenarios, namely, the 1998 El Niño and the 1999 La Niña. The major highlights are as follows:

- The MMF-simulated surface precipitation pattern agrees with TRMM estimates, especially in the nonrainy region. Compensating downward motion away from major precipitation centers was stronger and produced stronger warming and

drying in the MMF. This leads the MMF to simulate larger and more realistic nonraining regions.

- The MMF-simulated IWCs generally agree well with satellite (MLS) estimates in terms of the shape of the distribution. However, the MLS sensitivity limits its ability to detect the small and large IWCs that were simulated in the MMFs.

- The MMF-simulated diurnal variation of precipitation shows good agreement with merged microwave observations. For example, the MMF-simulated frequency maximum was in the late afternoon (1400–1800 LST) over land and in the early morning (0500–0700 LST) over the oceans. The fvGCM-simulated frequency maximum was too early for both oceans and land.

- The MMF-simulated MJO is stronger and shows eastward propagation. In contrast, the fvGCM-simulated MJO is very weak and the observed eastward-propagating MJO signals are nonexistent.

- Despite differences in model dynamics, coupling interfaces and physics between the Goddard and CSU MMFs, they both performed better against satellite observations than did their parent GCMs. However, both MMFs also simulated the positive precipitation bias (i.e., an over estimation of precipitation in the western Pacific). The positive precipitation bias could be due to the cyclic lateral boundary conditions, the two-dimensionality of the CRMs, localized convective–wind–evaporation feedback, stronger vertical upward motion, or a combination of factors.

- There are differences between the two MMFs. For example, the CSU MMF simulated less rainfall over land than its parent GCM. This is why the CSU MMF simulated less global rainfall than its parent GCM. The Goddard MMF, however, overestimates global rainfall because of its oceanic component.

- More detailed comparison of longer simulations (i.e., 10-yr integration) between Goddard and CSU MMFs' performance against satellite and ground-based observations will be needed, particularly for low-frequency modes (e.g., MJO and ENSO). In addition, a better design for future MMFs is needed and being developed (i.e., quasi 3D and global 2D). Major CRM-related issues (i.e., dynamics, microphysics, dimensionality, grid sizes, and land surface) were discussed ("Issues and future research" section).

The MMF is a natural extension of current CRM activities. MMFs can bridge the gap between tradi-

TABLE 5. A brief summary of the strengths and weaknesses of different modeling approaches.

Type of model (spatial scale)	Strengths	Weaknesses
GCMs (10^2 km)	Global coverage climate change assessment	Coarse-resolution cumulus parameterization
Regional-scale models (10^1–10^0 km)	Regional coverage, regional climate, better parameterization (nesting technology)	No feedback to global circulation case study
Cloud-resolving models (10^0–10^{-1} km)	Better physics, better treatment of cloud–radiation interaction	Small domain, no feedback to global circulation case study (field campaign)
Coupled GCM–CRM (MMF) (10^2–4 km)	Global coverage CRM-based physics	Computational cost, 2D CRM embedded (4-km grid)
Global cloud-resolving model (10^0 km)	Global coverage CRM-based physics	Computational cost, data management/analyses

tional CRM simulations, regional weather forecast models, and current and future nonhydrostatic global cloud–resolution models. The traditional CRM needs large-scale advective forcing in temperature and water vapor from intensive sounding networks deployed during major field experiments or from large-scale model analyses to be imposed as an external forcing (Soong and Ogura 1980; Soong and Tao 1980; Tao and Soong 1986; Lipps and Helmer 1986; and many others). The advantage of this approach is that the simulated rainfall, temperature, and water vapor budget are forced to be in good agreement with ob-servations (see Moncrieff et al. 1997; Moncrieff and Tao 1999; Randall et al. 2003b; Tao and Moncrieff 2003; Tao 2003, 2007 for review). However, there is no feedback from the CRM to the large-scale model (i.e., the CRM environment). In contrast, an MMF allows explicit interactions between the CRM and the GCM. With the traditional approach, CRMs can only examine the sensitivity of model grid size or physics for one type of cloud/cloud system at a single geo-graphic location. MMFs, however, could be used to identify the optimal grid size and physical processes (i.e., microphysics, cloud–radiation interaction) on a global scale. For example, MMFs can be used to iden-tify the optimal grid size and physical processes (i.e., microphysics, cloud–radiation interactions) needed for nonhydrostatic global CRMs (Satoh et al. 2005; Nasuno et al. 2008[4]). Regional forecast models [i.e., the Weather Research and Forecasting Model (WRF); Michalakes et al. 2001] can also be conducted in CRM mode and could cover large domains (i.e., a tropical channel model) through a two-way interactive nesting

technique. The physical processes developed/tested for CRMs could be also used for regional-scale models from idealized research to operational forecasting. It is expected that a close collaboration between CRMs, regional-scale models, MMFs, and nonhydrostatic high-resolution regional and global cloud-resolving models can enhance our ability to simulate realistic weather and climate in the near future. The strengths and weaknesses of different modeling approaches are summarized in Table 5.

APPENDIX A: BRIEF DESCRIPTIONS OF THE FVGCM, THE GCE, THE GODDARD MMF, THE CSU MMF, AND THE MMFS' COUPLING STRATEGY. *fvGCM*. The fvGCM has been constructed by combining the finite-volume dynamic core developed at Goddard (Lin 2004) with the physics package of the NCAR CCM3, which rep-resents a well-balanced set of processes with a long history of development and documentation (Kiehl et al. 1998). The unique features of the finite-volume

---

[4] This model is intended for high-resolution climate simula-tions and has been performed on an aquaplanet setup with grid intervals of 7 and 3.5 km for seasonal simulation (because of its extensive computation requirement and data storage).

dynamical core include an accurate conservative flux-form semi-Lagrangian transport algorithm (FFSL), with a monotonicity constraint on subgrid distributions that is free of Gibbs oscillation (Lin and Rood 1996, 1997); a physically consistent integration of the pressure gradient force for a terrain-following Lagrangian control-volume vertical coordinate (Lin 1997); and a mass-, momentum-, and total energy–conserving vertical remapping algorithm. The physical parameterizations of the fvGCM have been upgraded by incorporating the gravity wave drag scheme of the NCAR Whole Atmosphere Community Model (WACCM) and the CLM-2 (Bonan et al. 2002). This model has been applied in climate simulation, data assimilation, and high-resolution weather prediction modes (Atlas et al. 2005, 2007; Bloom et al. 2005; Shen et al. 2006a,b).

GCE model. The GCE model has been developed and improved at Goddard Space Flight Center over the past two and a half decades. The equations that govern cloud-scale motion (wind) in the GCE model are anelastic by filtering out sound waves. The subgrid-scale turbulence used in the GCE model is based on work by Klemp and Wilhelmson (1978). In their approach, one prognostic equation is solved for subgrid kinetic energy, which is then used to specify the eddy coefficients. The effect of condensation on the generation of subgrid-scale kinetic energy is also incorporated in the model (see Soong and Ogura 1980). The cloud microphysics includes a parameterized Kessler-type two-category liquid water scheme (cloud water and rain), and a three-category ice-phase scheme (cloud ice, snow, and hail/graupel) mainly based on Lin et al. (1983) and Rutledge and Hobbs (1984). However, there are several differences between the Goddard three-category ice-phase scheme and the Lin et al. (1983) and Rutledge and Hobbs (1984) schemes (see Tao et al. 2003). Recently, the sedimentation of falling ice crystals (Heymsfield and Iaquinta 2000) was included in the GCE model. Solar and infrared radiation parameterizations are also included in the model. All scalar variables use forward time differencing and a positive definite advection scheme with a nonoscillatory option (Smolarkiewicz and Grabowski 1990). The dynamic variables use a second-order accurate advection scheme and a leapfrog time integration (kinetic energy semiconserving method). A review of its development and the application of the GCE to better understand precipitation processes can be found in Tao and Simpson (1993), Simpson and Tao (1993), Tao et al. (2003), and Tao (2003).

A coupled fvGCM–GCE modeling system (Goddard MMF). A prototype fvMMF has been developed at Goddard and includes the fvGCM run at 2.5° × 2° horizontal grid spacing with 32 layers from the surface to 0.4 hPa and the two-dimensional (2D) GCE using 64 horizontal grids (in the east–west orientation) with 4-km grid spacing, 30 vertical levels, and cyclic lateral boundaries. The time step for the 2D GCE is 10 s, and the fvGCM-GCE coupling interval is 1 h (which is the fvGCM physical time step).

Because the vertical coordinate of the fvGCM (a terrain-following coordinate) is different from that of the GCE [a height (z) coordinate], vertical interpolations are needed in the coupling interface. An interpolation scheme, based on a finite-volume piecewise parabolic mapping (PPM) algorithm (Woodward and Colella 1984; Lin 2004), has been developed to conserve mass, momentum, and moist static energy between the two coordinates.

A coupled CAM–SAM modeling system (CSU MMF). The CRM used in the CSU MMF is the System for Atmospheric Modeling (SAM; Khairoutdinov and Randall 2003). It has 28 vertical layers, which are collocated with the lowest 28 levels in the parent GCM. The differences between the SAM and GCE model used in the Goddard MMF are the thermodynamic and microphysical processes. The prognostic thermodynamic variables in SAM include the liquid/ice water moist static energy, the total nonprecipitating water, and the total precipitating water. The mixing ratio of cloud water, cloud ice, rain, snow, and graupel are diagnosed from the prognostic variables by partitioning the liquid and ice phases as a function of temperature. Bulk microphysics is applied to compute the hydrometeor conversion rates and terminal velocities.

The GCM used in the CSU MMF is the NCAR CAM (Collins et al. 2006). CAM was configured to run at T42 horizontal resolution (~2.8° × 2.8° grid) using 30 levels with the top at 3.5 hPa. The CAM time step is 900 s. A semi-Largrangian dynamical core was used because of better scalability on massively parallel computers. Some of the physical parameterizations (i.e., radiation, grid-scale moist physics, and turbulent diffusion) used in CAM are improved versions of those in CCM3. The coupling time between CAM and SAM is 15 min. The SAM has 32 columns with 4-km resolution oriented in the north–south direction in the CSU MMF (Khairoutdinov et al. 2008). Table 1 lists the major characteristics of the MMFs developed at CSU and NASA Goddard.

MMFs' coupling strategy. The coupling between the fvGCM and GCE is identical to the CSU MMF (Khairoutdinov et al. 2005). The GCE model continuously integrates its equations for the duration of the fvGCM time step and is continuously forced by the large-scale tendencies computed as

$$\left(\frac{\partial \phi}{\partial t}\right)_{LS} = \frac{\phi_{LS} - \overline{\phi}^{n}}{\Delta t_{LS}}, \tag{A1}$$

where ϕ denotes any prognostic GCE model variables (i.e., temperature, water vapor mixing ratio), ϕ_{LS} denotes the corresponding variable computed by the fvGCM as a result of all of the large-scale processes before the GCE model call at the current fvGCM time step, and $\overline{\phi}^{n}$ is the horizontally averaged GCE model variable at the end of the GCE model call at the previous fvGCM time step Δt_{LS}. With this coupling, the large-scale forcing mainly acts to relax the GCE model horizontal averages to the provisional fvGCM field. By design, the forcing term (A1) does not allow systematic "drift" of the GCE mean fields away from the corresponding fvGCM fields. The GCE returns the large-scale tendencies resulting from the GCE processes, which are computed as

$$\left(\frac{\partial \phi}{\partial t}\right)_{CRM} = \frac{\overline{\phi}^{n+1} - \phi_{LS}}{\Delta t_{LS}}, \tag{A2}$$

where $\overline{\phi}^{n+1}$ is the horizontal mean of the GCE-modeled fields at the end of the GCE model call. The forcing term in (A1) ensures that in the absence of cloud processes or convection resolved by the GCE model domain, $\overline{\phi}^{n+1}$ will be identical to ϕ_{LS} at the end of GCE model call, thus producing zero tendencies resulting from subgrid processes.

Note that this coupling strategy does not include dynamic feedback (i.e., momentum transport) from the CRM to its parent GCM. Also, only a 2D version of the CRM is used. In addition, cloud-scale cloud–radiation and cloud–surface processes have not been included; instead, the radiative transfer and surface fluxes were computed on the GCM grids using average profiles of cloud properties simulated by the CRMs.

REFERENCES

Arakawa, A., 2004: The cumulus parameterization problem: Past, present, and future. *J. Climate,* **17,** 2493–2525.

Atlas, R., and Coauthors, 2005: Hurricane forecasting with the high-resolution NASA finite volume general circulation model. *Geophys. Res. Lett.,* **32,** L03801, doi:10.1029/2004GL021513.

——, S.-J. Lin, B.-W. Shen, O. Reale, and K.-S. Yeh, 2007: Improving hurricane prediction through innovative global modeling. *Extending the Horizons: Advances in Computing, Optimization, and Decision Technologies,* E. K. Baker et al., Springer, 1–14.

Betts, A. K., and C. Jakob, 2002: Study of diurnal cycle of convective precipitation over Amazonia using single column model. *J. Geophys. Res.,* **107,** 4732, doi:10.1029/2002JD002264.

Bloom, S., and Coauthors, 2005: Documentation and validation of the Goddard Earth Observing System (GEOS) Data Assimilation System—Version 4. Technical Report Series on Global Modeling and Data Assimilation, Vol. 26, NASA/TM-2005-104606, 181 pp.

Bonan, G. B., K. W. Oleson, M. Vertenstein, S. Levis, X. Zeng, Y. Dai, R. E. Dickinson, and Z.-L. Yang, 2002: The land surface climatology of the Community Land Model coupled to the NCAR Community Climate Model. *J. Climate,* **15,** 3123–3149.

Cheng, A., and K.-M. Xu, 2006: Simulation of shallow cumuli and their transition to deep convective clouds by cloud-resolving models with different third-order turbulence closures. *Quart. J. Roy. Meteor. Soc.,* **132,** 359–382.

Chou, M.-D., and M. J. Suarez, 1999: A solar radiation parameterization for atmospheric studies. NASA Tech. Rep. NASA TM-1999-10460, Vol. 15, 38 pp.

——, and ——, 2001: A thermal infrared radiation parameterization for atmospheric studies. NASA Tech. Ref. NASA/TM-2001-104606, Vol. 19, 55 pp.

Collins, W. D., and Coauthors, 2006: The formulation and atmospheric simulation of the Community Atmosphere Model Version 3. *J. Climate,* **19,** 2144–2161.

Das, S., D. Johnson, and W.-K. Tao, 1999: Single-column and cloud ensemble model simulations of TOGA COARE convective systems. *J. Meteor. Soc. Japan,* **77,** 803–826.

GEWEX Cloud System Science Team, 1993: The GEWEX Cloud System Study (GCSS). *Bull. Amer. Meteor. Soc.,* **74,** 387–399.

Grabowski, W. W., 2001: Coupling cloud processes with the large scale dynamics using the cloud resolving convection parameterization (CRCP). *J. Atmos. Sci.,* **58,** 978–997.

——, 2003: MJO-like coherent structures: Sensitivity simulations using the cloud-resolving convection parameterization (CRCP). *J. Atmos. Sci.,* **60,** 847–864.

——, and P. K. Smolarkiewicz, 1999: CRCP: A cloud resolving convective parameterization for modeling

the tropical convective atmosphere. *Physica,* **133,** 171–178.

——, X. Wu, M. W. Moncrieff, and W. D. Hall, 1998: Cloud resolving modeling of tropical cloud systems during PHASE III of GATE. Part II: Effects of resolution and the third dimension. *J. Atmos. Sci.,* **55,** 3264–3282.

Guichard, F., and Coauthors, 2004: Modeling the diurnal cycle of deep precipitating convection over land with cloud-resolving and single-column models. *Quart. J. Roy. Meteor. Soc.,* **130,** 3139–3172.

Heymsfield, A. J., and J. Iaquinta, 2000: Cirrus crystal terminal velocities. *J. Atmos. Sci.,* **57,** 916–938.

Khairoutdinov, M. F., and Y. L. Kogan, 1999: A large-eddy simulation model with explicit microphysics: Validation against aircraft observations of a stratocumulus-topped boundary layer. *J. Atmos. Sci.,* **56,** 2115–2131.

——, and D. A. Randall, 2001: A cloud resolving model as a cloud parameterization in the NCAR community climate system model: Preliminary results. *Geophys. Res. Lett.,* **28,** 3617–3620.

——, and ——, 2003: Cloud resolving modeling of the ARM summer 1997 IOP: Model formulation, results, uncertainties, and sensitivities. *J. Atmos. Sci.,* **60,** 607–625.

——, ——, and C. A. DeMott, 2005: Simulations of the atmospheric general circulation using a cloud-resolving model as a superparameterization of physical processes. *J. Atmos. Sci.,* **62,** 2136–2154.

——, C. A. DeMott, and D. A. Randall, 2008: Evaluation of the simulated interannual and subseasonal variability in an AMIP-style simulation using the CSU Multiscale Modeling Framework. *J. Climate,* **21,** 413–431.

Kiehl, J. T., J. J. Hack, G. B. Bonan, B. A. Boville, D. L. Williamson, and P. J. Rasch, 1998: The National Center for Atmospheric Research Community Climate Model: CCM3. *J. Climate,* **11,** 1131–1150.

Klemp, J. B., and R. Wilhelmson, 1978: The simulation of three-dimensional convective storm dynamics. *J. Atmos. Sci.,* **35,** 1070–1096.

Knutson, T. R., and K. M. Weickmann, 1987: 30–60-day atmospheric oscillations: Composite life cycles of convection and circulation anomalies. *Mon. Wea. Rev.,* **115,** 1407–1436.

Kumar, S. V., and Coauthors, 2006: Land Information System—An interoperable framework for high resolution land surface modeling. *Environ. Modell. Software,* **21,** 1402–1415.

Kummerow, C., and Coauthors, 2001: The evolution of the Goddard profile algorithm (GPROF) for rainfall estimation from passive microwave sensors. *J. Appl.*

Meteor., **40,** 1801–1820.

Lang, S., W.-K. Tao, R. Cifelli, W. Olson, J. Halverson, S. Rutledge, and J. Simpson, 2007: Improving simulations of convective system from TRMM LBA: Easterly and westerly regimes. *J. Atmos. Sci.,* **64,** 1141–1164.

Liang, X.-Z., and X. Wu, 2005: Evaluation of a GCM subgrid cloud-radiation interaction parameterization using cloud-resolving model simulations. *Geophys. Res. Lett.,* **32,** L06801, doi:10.1029/2004GL022301.

Lin, S.-J., 1997: A finite-volume integration method for computing pressure gradient forces in general vertical coordinates. *Quart. J. Roy. Meteor. Soc.,* **123,** 1749–1762.

——, 2004: A "vertically Lagrangian" finite-volume dynamical core for global models. *Mon. Wea. Rev.,* **132,** 2293–2307.

——, and R. B. Rood, 1996: Multidimensional flux-form semi-Lagrangian transport schemes. *Mon. Wea. Rev.,* **124,** 2046–2070.

——, and ——, 1997: An explicit flux-form semi-Lagrangian shallow water model on the sphere. *Quart. J. Roy. Meteor. Soc.,* **123,** 2477–2498.

Lin, X., D. A. Randall, and L. D. Fowler, 2000: Diurnal variability of the hydrological cycle and radiative fluxes: Comparisons between observations and a GCM. *J. Climate,* **13,** 4159–4179.

——, S. Q. Zhang, and A. Y. Hou, 2007: Variational assimilation of global microwave rainfall retrievals: Physical and dynamical impact on GEOS analyses. *Mon. Wea. Rev.,* **135,** 2931–2957.

Lin, Y.-L., R. D. Farley, and H. D. Orville, 1983: Bulk parameterization of the snow field in a cloud model. *J. Climate Appl. Meteor.,* **22,** 1065–1092.

Lipps, F. B., and R. S. Helmer, 1986: Numerical simulation of deep tropical convection associated with large-scale convergence. *J. Atmos. Sci.,* **43,** 1796–1816.

Luo, Z., and G. L. Stephens, 2006: An enhanced convection-wind-evaporation feedback in a superparameterization GCM (SP-GCM) depiction of the Asian summer monsoon. *J. Geophys. Lett.,* **33,** L06707, doi:10.1029/2005GL025060.

Madden, R. A., and P. R. Julian, 1972: Description of global-scale circulation cells in the tropics with a 40-50 day period. *J. Atmos. Sci.,* **29,** 1109–1123.

——, and ——, 1994: Observations of the 40-50-day tropical oscillation—A review. *Mon. Wea. Rev.,* **122,** 814–837.

McCumber, M., W.-K. Tao, J. Simpson, R. Penc, and S.-T. Soong, 1991: Comparison of ice-phase microphysical parameterization schemes using numerical simulations of convection. *J. Appl. Meteor.,* **30,** 987–1004.

Michalakes, J., S. Chen, J. Dudhia, L. Hart, J. Klemp, J. Middecoff, and W. Shamarock, 2001: Development

of a next-generation regional weather research and forecast model. Tech. Note Argonne National Laboratory Publication ANL/MCSP868-0101, 8 pp.

Moncrieff, M. W., and W.-K. Tao, 1999: Cloud-resolving models. *Global Water and Energy Cycles,* K. Browing and R. J. Gurney, Eds., Cambridge University Press, 200–209.

——, S. K. Krueger, D. Gregory, J.-L. Redelsperger, and W.-K. Tao, 1997: GEWEX Cloud System Study (GCSS) Working Group 4: Precipitating convective cloud systems. *Bull. Amer. Meteor. Soc.,* **78,** 831–845.

Nasuno, T., H. Tomita, S. Iga, H. Miura, and M. Satoh, 2008: Multi-scale organization of convection simulated with explicit cloud processes on an aquaplanet. *J. Atmos. Sci.,* **65,** 1246–1265.

Ogura, Y., and N. A. Phillips, 1962: Scale analysis of deep and shallow convection in the atmosphere. *J. Atmos. Sci.,* **19,** 173–179.

Oleson, K. W., and Coauthors, 2004: Technical description of the Community Land Model (CLM). NCAR Tech. Rep. NCAR/TN-461STR, 174 pp.

Pincus, R., H. W. Baker, and J.-J. Mocrette, 2003: A fast, flexible, approximation technique for computing radiative transfer in inhomogeneous cloud fields. *J. Geophys. Res.,* **108,** 4376, doi:10.1029/2002JD003322.

Randall, D. A., Harshvardhan, and D. A. Dazlich, 1991: Diurnal variability of the hydrologic cycle in a general circulation model. *J. Atmos. Sci.,* **48,** 40–62.

——, M. Khairoutdinov, A. Arakawa, and W. Grabowski, 2003a: Breaking the cloud parameterization deadlock. *Bull. Amer. Meteor. Soc.,* **84,** 1547–1564.

——, and Coauthors, 2003b: Confronting models with data: The GEWEX Cloud Systems Study. *Bull. Amer. Meteor. Soc.,* **84,** 455–469.

Reynolds, R. W., N. A. Rayner, T. M. Smith, D. C. Stokes, and W. Wang, 2002: An improved in situ and satellite SST analysis for climate. *J. Climate,* **15,** 1609–1625.

Rutledge, S. A., and P. V. Hobbs, 1984: The mesoscale and microscale structure and organization of clouds and precipitation in mid-latitude clouds. Part XII: A diagnostic modeling study of precipitation development in narrow cold frontal rainbands. *J. Atmos. Sci.,* **41,** 2949–2972.

Satoh, M., H. Tomita, H. Miura, S. Iga, and T. Nasuno, 2005: Development of a global cloud resolving model—A multi-scale structure of tropical convections. *J. Earth Simulator,* **3,** 1–9.

Shen, B.-W., R. Atlas, J.-D. Chern, O. Reale, S.-J. Lin, T. Lee, and J. Chang, 2006a: The finite volume general mesoscale circulation model on the NASA Columbia supercomputer: 0.125 degree Preliminary simulations of mesoscale vortices. *Geophys. Res. Lett.,* **33,** L05801, doi:10.1029/2005GL024594.

——, ——, O. Oreale, S.-J. Lin, J.-D. Chern, J. Chang, C. Henze, and J.-L. Li, 2006b: Hurricane forecasts with a global mesoscale-resolving model: Preliminary results with Hurricane Katrina (2005). *Geophys. Res. Lett.,* **33,** L13813, doi:10.1029/2006GL026143.

Simpson, J., and W.-K. Tao, 1993: The Goddard Cumulus Ensemble Model. Part II: Applications for studying cloud precipitating processes and for NASA TRMM. *Terr. Atmos. Oceanic Sci.,* **4,** 73–116.

——, R. F. Adler, and G. North, 1988: A proposed Tropical Rainfall Measuring Mission (TRMM) satellite. *Bull. Amer. Meteor. Soc.,* **69,** 278–295.

——, C. Kummerow, W.-K. Tao, and R. F. Adler, 1996: On the Tropical Rainfall Measuring Mission (TRMM). *Meteor. Atmos. Phys.,* **60,** 19–36.

Slingo, A., R. C. Wilderspin, and S. J. Brentnall, 1987: Simulation of the diurnal cycle of outgoing longwave radiation with an atmospheric GCM. *Mon. Wea. Rev.,* **115,** 1451–1457.

Smolarkiewicz, P. K., and W. W. Grabowski, 1990: The multidimensional positive advection transport algorithm: Nonoscillatory option. *J. Comput. Phys.,* **86,** 355–375.

Soong, S.-T., and Y. Ogura, 1980: Response of trade wind cumuli to large-scale processes. *J. Atmos. Sci.,* **37,** 2035–2050.

——, and W.-K. Tao, 1980: Response of deep tropical clouds to mesoscale processes. *J. Atmos. Sci.,* **37,** 2016–2036.

Sui, C.-H., K.-M. Lau, Y. Takayabu, and D. Short, 1997: Diurnal variations in tropical oceanic cumulus convection during TOGA COARE. *J. Atmos. Sci.,* **54,** 637–655.

——, X. Li, K.-M. Lau, W.-K. Tao, M.-D. Chou, and M.-J. Yang, 2008: Convective-radiative-mixing processes in the tropical ocean-atmosphere. *Recent Progress in Atmospheric Sciences: Applications,* K.-N. Liou and M.-D. Chou, Eds., World Scientific, 66–88.

Tao, W.-K., 2003: Goddard Cumulus Ensemble (GCE) model: Application for understanding precipitation processes. *Cloud Systems, Hurricanes and the Tropical Rainfall Measuring Mission (TRMM): A Tribute to Dr. Joanne Simpson, Meteor. Monogr.* No. 51, Amer. Meteor. Soc., 103–138.

——, 2007: Cloud resolving modeling. *J. Meteor. Soc. Japan,* **85,** 305–330.

——, and S.-T. Soong, 1986: A study of the response of deep tropical clouds to mesoscale processes: Three-dimensional numerical experiments. *J. Atmos. Sci.,* **43,** 2653–2676.

——, and J. Simpson, 1993: The Goddard Cumulus Ensemble Model. Part I: Model description. *Terr. Atmos. Oceanic Sci.,* **4,** 19–54.

——, and M. Moncrieff, 2003: Cloud modeling. *Encyclopedia of Atmospheric Sciences,* J. Holton, J. Curry, and J. Pyle, Eds., Academic Press, 539–548.

——, J. Simpson, and S.-T. Soong, 1987: Statistical properties of a cloud ensemble: A numerical study. *J. Atmos. Sci.,* **44,** 3175–3187.

——, S. Lang, J. Simpson, C.-H. Sui, B. Ferrier, and M.-D. Chou, 1996: Mechanisms of cloud-radiation interaction in the tropics and midlatitudes. *J. Atmos. Sci.,* **53,** 2624–2651.

——, and Coauthors, 2003: Microphysics, radiation and surface processes in a non-hydrostatic model. *Meteor. Atmos. Phys.,* **82,** 97–137.

Woodward, P. R., and P. Colella, 1984: The numerical simulation of two-dimensional fluid flow with strong shocks. *J. Comput. Phys.,* **54,** 115–173.

Wu, X., and X.-Z. Liang, 2005: Effect of sub-grid cloud-radiation interaction on climate simulations. *Geophys. Res. Lett.,* **32,** L24806, doi:10.1029/2005GL024432.

——, ——, G. J. Zhang, 2003: Seasonal migration of ITCZ precipitation across the equator: Why can't GCMs simulate it? *Geophys. Res. Lett.,* **30,** 1824, doi:10.1029/2003GL017198.

——, L. Deng, X. Song, and G. J. Zhang, 2007: Coupling of convective momentum transport with convective heating in global climate simulations. *J. Atmos. Sci.,* **64,** 1334–1349.

Xie, S., and Coauthors, 2005: Simulations of mid-latitude frontal clouds by single-column and cloud-resolving models during the Atmospheric Radiation Measurement March 2000 cloud intensive operational period. *J. Geophys. Res.,* **110,** D15S03, doi:10.1029/2004JD005119.

Yang, G.-Y., and J. Slingo, 2001: The diurnal cycle in the tropics. *Mon. Wea. Rev.,* **129,** 784–801.

Zeng, X., and Coauthors, 2007: Evaluating clouds in long-term cloud-resolving model simulations with observational data. *J. Atmos. Sci.,* **64,** 4153–4177.

Zhang, G. J., 2002: Convective quasi-equilibrium in midlatitude continental environment and its effect on convective parameterization. *J. Geophys. Res.,* **107,** doi:10.1029/2001JD001005.

——, and X. Wu, 2003: Convective momentum transport and perturbation pressure field from a cloud-resolving model simulation. *J. Atmos. Sci.,* **60,** 1120–1139.

Zhang, Y. C., W. B. Rossow, A. A. Lacis, V. Oinas, and M. I. Mishchenko, 2004: Calculation of radiative fluxes from the surface to top of atmosphere based on ISCCP and other global data sets: Refinements of the radiative transfer model and the input data. *J. Geophys. Res.,* **109,** D19105, doi:10.1029/2003JD004457.